Journal of Applied Physics ARTICLE scitation.org/journal/jap

Theory of asymmetric and piezotronically modified double Schottky barriers

Cite as: J. Appl. Phys. **132**, 145702 (2022); doi: 10.1063/5.0095686
Submitted: 12 April 2022 · Accepted: 8 September 2022 ·
Published Online: 13 October 2022

Benjamin Kaufmann[1,a)] and Peter Supancic[1,2]

AFFILIATIONS

[1]Department of Materials Science, Montanuniversität Leoben, Franz Josef-Straße 18, 8700 Leoben, Austria
[2]Materials Center Leoben Forschung GmbH, Roseggerstraße 12, 8700 Leoben, Austria

[a)]**Author to whom correspondence should be addressed:** benjamin.kaufmann@posteo.de

ABSTRACT

We present a theoretical model for double Schottky barriers at zinc oxide grain boundaries that accounts for piezotronically modified barrier heights resulting in generally asymmetric current–voltage (I–V) characteristics with respect to the applied electrical field direction. The model is based on charge distributions in the vicinity of the barrier and its related electrical potential distributions and can be considered as a generalization of the famous model of Blatter and Greuter. The natural asymmetry of current with respect to forward and reverse bias can be explained by different grain orientations and donor densities. The previously experimentally found change of I–V curves due to the application of mechanical loads can be reproduced via the piezotronic effect, leading to changes in the barrier potential profile due to piezoelectrically induced surface charges. Also, the I–V characteristics of degraded grain boundaries can be interpreted in terms of asymmetric changes in the donor densities. In addition, a second approach is presented that is able to explain experimental data of asymmetric I–V curves of wide grain boundaries with different surface terminations (O and Zn-polar).

I. INTRODUCTION

It is well known that in semiconducting polycrystalline ZnO, doped with certain metal oxides, a negative charge can accumulate at the grain boundaries (GBs). This charge leads to electrostatic potential barriers, the so-called double Schottky barriers (DSBs) that give the ceramic a strongly nonlinear voltage-dependent resistance and make it a very prominent material for surge arresters, also referred to as metal oxide varistors (*var*iable re*sistors*). The varistor effect of ZnO has been known since the last 50 years[1] and it is described by theories of the current across DSBs established between 1979 and 1990.[2–5] More recently, ZnO came into the focus of research due to the influence of the piezoelectric properties on its semiconducting properties and has thereby contributed significantly to establishing the field of "piezotronics."[6–9] Among the tetrahedrally bonded semiconductors, ZnO has the highest piezoelectric constants, promising strong electromechanical coupling, which has been demonstrated, for example, for metal/ZnO Schottky contacts where it was found that strain can cause a shift in Schottky barrier height.[10–13]

Piezotronic effects can also be observed in ZnO varistors[14] and have been investigated thoroughly in recent years.[12,15–21] These studies show that piezoelectrically induced surface charges can, due to mechanical stress, manipulate the charge in the GB and, thus, the barrier height of the DSB, making the electrical conductivity of the material highly sensitive to applied pressure.[18]

Although the effect of pressure on ZnO varistors has been known since the 1970s,[22–24] it was not until 2000 that this effect could be attributed to piezoelectricity by Verghese and Clarke.[14]

Later, in 2014, Baraki *et al.*[16] adopted the model of Verghese and Clarke and implemented it in the until this day accepted theory of current across ZnO GBs of Blatter and Greuter[3–5] and proposed that the voltage-dependent DSB height ϕ_b (here in units of energy) can be described by

$$\phi_b = \frac{\left((Q_i + Q_p)^2 - 2e\varepsilon NV\right)^2}{8\varepsilon N(Q_i + Q_p)^2}, \tag{1}$$

where Q_i is the interface surface charge (per area) in the GB due to occupied acceptor states for electrons, Q_p is the piezoelectrically induced net surface charge (i.e., the sum of the contributions of both neighboring grains), e is the elementary charge, ε is the

absolute permittivity of the ZnO grains, N is the number of ionized donors per volume in the space charge region (the depletion region) at the GB, and V is the applied voltage (i.e., the difference in electric potential between the two grains).

The electrical behavior of individual GBs under mechanical stress was investigated experimentally by previous works[17,19–21] and Eq. (1) could be confirmed for symmetric GBs of ZnO bicrystals.[19] In this context, a GB is said to be "symmetric" if the contributions to the net induced piezoelectric charge are the same for both surfaces of the two grains forming the GB.

For asymmetric GBs, which is the typical case in ZnO microstructures with random orientations of the polar axes of the crystal grains, the contributions of piezoelectric charges of the grains at the DSB can be strongly different, even the sign of the charge. Depending on the grain orientations and the applied pressure, the DSB height seems to increase at one side and decreases at the other side, causing an asymmetric current–voltage (I–V) characteristic of the GB, i.e., the forward and reverse I–V curves differ,[17,21] a phenomenon that was not considered in the work of Verghese and Clarke in 2000.[14] According to Verghese and Clarke, the DSB height is the same for both current direction and is only dependent on the total charge in the GB, which is the sum of the interface charge and the piezoelectrically induced surface charge, as described by Eq. (1).

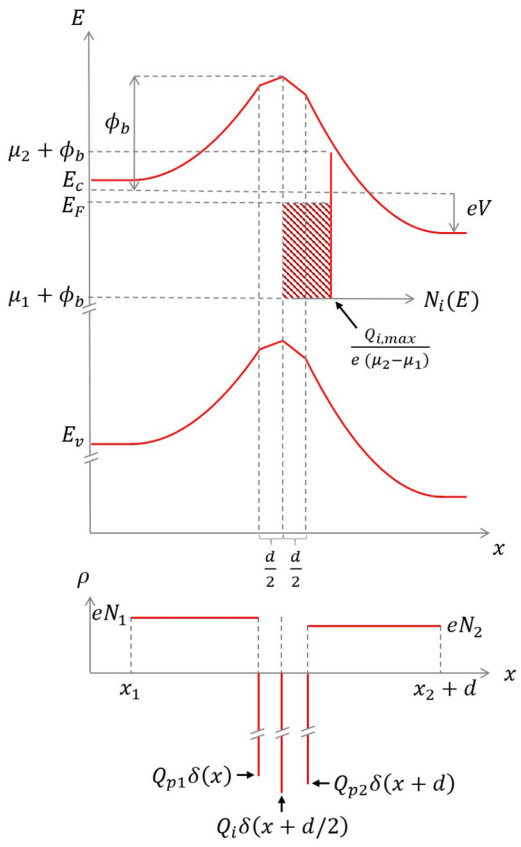

FIG. 1. Simplified energy-band diagram and charge distribution of an asymmetric double Schottky barrier.

Asymmetric I–V behavior of ZnO GBs, where the forward and reverse I–V curves differ, has been documented in several papers.[21,25–28] In 1995, Wang *et al.*[25] reported asymmetric I–V curves of individual GB whose pre-breakdown current and asymmetry increased after long-term (15 h) electrical (5.7 V at ∼ 40 μA) and thermal (100 °C) load. Although the degradation (the increase in pre-breakdown current) of ZnO DSBs is now broadly understood to be caused by ion migration,[29] the associated increase in asymmetry is still unresolved. An explanation for asymmetric I–V characteristics was put forward by Cheng *et al.*[27] who introduced a dipole model of the GB and explained the asymmetric I–V behavior of ZnO bicrystals as caused by different surface polarities of the O and Zn-terminated crystal faces. Raidl *et al.*[17] used the dipole ansatz of Cheng *et al.* to describe asymmetric I–V curves of piezotronically modified DSBs in low-voltage varistors. Billovits *et al.*[21] confirmed the claims of this approach. Although the experimental results could be explained phenomenologically correctly, the dipole approach of Cheng *et al.* left a noticeable flaw: It assumes that there are two different barrier heights, one for each grain surface. It remains unclear why electrons moving through the GB have to overcome only one of these barriers. It can be safely assumed that an electron must always overcome the peak of the electrostatic potential, regardless of which side the electron comes from.

In the present work, the model of Blatter and Greuter from 1986,[3] which is still considered as the correct theory of DSBs (but which deals only with symmetric GBs), is extended to asymmetric GBs by introducing a dipole moment induced by surface charges on the grains and by considering different ionized donors and permittivities (grain orientations) of the two grains forming the GB. As will be shown, the resulting theory is capable of explaining the observed phenomena: the asymmetry due to piezotronically modified DSBs and the asymmetry due to degraded GBs. The asymmetry due to differing surface terminations as documented by Cheng *et al.*,[27] however, requires a slightly different approach, which is explained by the fact that their experimental data come from measurements on bicrystals with relatively thick (∼25 μm) and presumably conductive GBs.

II. THEORY

The presented theory of asymmetric and piezotronically modified DSBs is based on Blatter and Greuter's model (BGM)[3] who idealized the GB as an (infinitely thin) negative surface charge, mathematically treated as a Dirac delta distribution. This surface charge builds up an electrostatic potential that repels the mobile electrons in the grains in the vicinity of the GB, resulting in depletion regions at the GB. In an energy-band diagram, this is represented by an upward bending of the electron bands. The BGM is a symmetric model, i.e., when no voltage is applied, the band-bending is symmetric at the GB. The reason for this symmetry is that the two grains have the same properties, such as the same donor densities and the same permittivities, resulting in symmetric current–voltage (I–V) curves (forward and reverse absolute currents are equal for the same applied voltage). However, the donor density of real GBs can vary from grain to grain[29] and the permittivity can also differ due to the direction-dependent dielectric

constant of ZnO.[30] Furthermore, there can be an electric dipole moment at the GB due to different surface charges of the grains (piezocharge, surface termination, etc.). This can lead to asymmetric I–V behavior, which was not considered by Blatter and Greuter.

We extended the BGM by introducing a possible dipole moment at the GB caused by different piezoelectric and/or polarization surface charges Q_{p1} and Q_{p2} (Fig. 1) and also considered the effects of different donor densities and permittivities (different crystal/grain orientations). The interface dipole moment is defined as

$$p_i = d(Q_{p1} - Q_{p2}), \tag{2}$$

with d the spatial separation of the grain surface charges Q_{p1} and Q_{p2} (charge per area). d can be regarded as the thickness of the GB. The dipole causes an energy gap ep_i/ε_i between the left and right electron band of the grains [Fig. 2(b)], with ε_i being the absolute permittivity of the interface (the GB).

The charge distribution [Fig. 2(a)] is modeled by

$$\rho(x) = eN_1[\Theta(x - x_1) - \Theta(x)] + eN_2[\Theta(x) - \Theta(x - x_2)] + (Q_i + Q_{p1} + Q_{p2})\delta(x) + p_i\delta'(x). \tag{3}$$

N_1 and N_2 are the densities of shallow donors of the grains (the donor densities per volume). Q_i is the surface charge (charge per area) due to acceptor states in the GB. $p_{1,2}$ represents the dipole moment as defined in Eq. (2). $\Theta(x)$ is the Heaviside step function, $\delta(x)$ is the Dirac delta distribution and $\delta'(x)$ denotes its derivation.

Solving Poisson's equation,

$$\frac{d^2}{dx^2}\varphi(x) = -\frac{\rho(x)}{\varepsilon(x)}, \tag{4}$$

with the absolute permittivity

$$\varepsilon(x) = \varepsilon_1\Theta(-x) + \varepsilon_2\Theta(x) + \varepsilon_i\delta(x), \tag{5}$$

where ε_1 and ε_2 are the permittivities of the left and right grain, we obtained for the electric potential [Fig. 2(b)],

$$\varphi(x) = \begin{cases} 0 & \text{if } x \le x_1, \\ -\dfrac{eN_1(x - x_1)^2}{2\,\varepsilon_1} & \text{if } x_1 \le x \le 0, \\ V - \dfrac{eN_2(x - x_2)^2}{2\,\varepsilon_2} & \text{if } 0 \le x \le x_2, \\ V & \text{if } x_2 \le x. \end{cases} \tag{6}$$

x_1 and x_2 are the points to where the depletion regions in the grains reach and V is the applied voltage (the difference in electric potential between grain 1 and grain 2, where the potential at grain 1 is defined to be zero).

The DSB height ϕ_b is defined as the maximum of the electrostatic potential that the electrons have to overcome (from the Fermi level) to move across the GB. A derivation of ϕ_b is given in the Appendix. Here, only the result is presented. We found that the products of dielectric constant and donor density ε_1N_1 and ε_2N_2 play a crucial role. There are two different solutions for the barrier height ϕ_b: one for the case $\varepsilon_1N_1 = \varepsilon_2N_2$,

$$\phi_b = \begin{cases} eV + \dfrac{\left((Q_i + Q_{p1} + Q_{p2})^2 - 2e\varepsilon_1N_1(V + p_i/\varepsilon_i)\right)^2}{8\varepsilon_1N_1(Q_i + Q_{p1} + Q_{p2})^2} & \text{if } V \le 0, \\ \dfrac{\left((Q_i + Q_{p1} + Q_{p2})^2 - 2e\varepsilon_1N_1(V + p_i/\varepsilon_i)\right)^2}{8\varepsilon_1N_1(Q_i + Q_{p1} + Q_{p2})^2} & \text{if } V \ge 0, \end{cases} \tag{7}$$

and another for the case $\varepsilon_1N_1 \neq \varepsilon_2N_2$,

$$\phi_b = \begin{cases} eV + \dfrac{e^2N_1}{2\,\varepsilon_1}\left\{\dfrac{\varepsilon_1(Q_i + Q_{p1} + Q_{p2})}{e\,(\varepsilon_1N_1 - \varepsilon_2N_2)} \pm \sqrt{\dfrac{N_2}{N_1}\dfrac{\varepsilon_1\varepsilon_2}{e\,(\varepsilon_1N_1 - \varepsilon_2N_2)}\left[\dfrac{(Q_i + Q_{p1} + Q_{p2})^2}{e\,(\varepsilon_1N_1 - \varepsilon_2N_2)} + 2V + 2\dfrac{p_i}{\varepsilon_i}\right]}\right\}^2 & \text{if } V \le 0, \\ \dfrac{e^2N_1}{2\,\varepsilon_1}\left\{\dfrac{\varepsilon_1(Q_i + Q_{p1} + Q_{p2})}{e\,(\varepsilon_1N_1 - \varepsilon_2N_2)} \pm \sqrt{\dfrac{N_2}{N_1}\dfrac{\varepsilon_1\varepsilon_2}{e\,(\varepsilon_1N_1 - \varepsilon_2N_2)}\left[\dfrac{(Q_i + Q_{p1} + Q_{p2})^2}{e\,(\varepsilon_1N_1 - \varepsilon_2N_2)} + 2V + 2\dfrac{p_i}{\varepsilon_i}\right]}\right\}^2 & \text{if } V \ge 0, \end{cases} \tag{8}$$

where the plus sign in front of the square root has to be applied for $\varepsilon_1N_1 > \varepsilon_2N_2$ and the minus sign for $\varepsilon_1N_1 < \varepsilon_2N_2$. It may be surprising that the formulas for ϕ_b look so different for the cases $\varepsilon_1N_1 = \varepsilon_2N_2$ and $\varepsilon_1N_1 \neq \varepsilon_2N_2$, as one would expect that the case $\varepsilon_1N_1 \neq \varepsilon_2N_2$ for the limit $\varepsilon_1N_1 \to \varepsilon_2N_2$ must pass into the case $\varepsilon_1N_1 \to \varepsilon_2N_2$. It is not obvious at first sight, but it does, as proved in the Appendix.

In Table I, the results for the DSB height are compared with the BGM[3] and the model of Verghese and Clarke.[14] The model of Verghese and Clarke contains the BGM for the case $Q_p = 0$. The

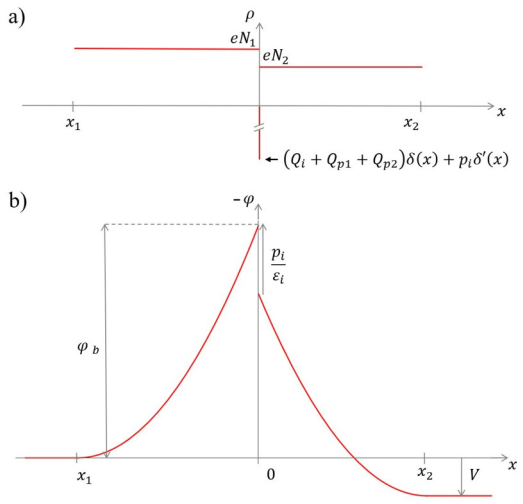

FIG. 2. (a) Simplified model of the charge density of a double Schottky barrier; (b) the electric potential at the grain boundary.

model presented here contains the model of Verghese and Clarke for the case $p_i = 0$ and $\varepsilon_1 N_1 = \varepsilon_2 N_2$. If, however, $p_i \neq 0$, the barrier height is asymmetric with respect to the applied voltage V. It is also asymmetric if $\varepsilon_1 N_1 \neq \varepsilon_2 N_2$.

With Eqs. (7) and (8), the DSB height is defined and the current density across a GB can be calculated from[27]

$$J_{GB}(V) = A^{*}\, T^2 \exp\left(-\frac{e\,\phi_b + \varepsilon_\xi}{k_B T}\right)\left[1 - \exp\left(-\frac{e\,V}{k_B T}\right)\right], \quad (9)$$

with A^{*}=32 A cm^{-2} K^{-2} being the Richardson constant of ZnO, T being the temperature at the GB, $\varepsilon_\xi = E_C - E_F = 0.067$ eV[3] being the difference between the conduction band minimum E_C and the Fermi level E_F, k_B being Boltzmann's constant, and V being the applied voltage.

Equation (9) [formula (3) in Ref. 27] is a simplification of the approach of the BGM [formula (11) in Ref. 3], where the electron capture probability in the GB is neglected. It only accounts for thermionic current as was proposed by Blatter and Greuter.[3,4]

The current over the DSB is dependent on the applied voltage and the barrier height. If the interface charge Q_i is not dependent on V, Eqs. (7) and (8) can specify the barrier height for any applied voltage $V_{c2} \leq V \leq V_{c1}$. However, it was the ground breaking approach of Pike and Seager[2] [later also used by Blatter and Greuter[3–5]] that could successfully describe the barrier breakdown by introducing a voltage-dependent Q_i that leads to an inhibited reduction of the barrier. According to this approach, the barrier height is also dependent on the applied voltage and the interface charge $Q_i + Q_{p1} + Q_{p2}$.

Q_i (the charge due to acceptor states) depends on the barrier height [formula (7) in Ref. 3],

$$Q_i(\phi_b) = e \int dE\, N_i(E, \phi_b) f(E), \quad (10)$$

where the Fermi–Dirac distribution is

$$f(E) = 1 \Big/ \left[1 + \exp\left(\frac{E - E_F}{k_B T}\right)\right]. \quad (11)$$

In contrast to the BGM, here the interface Fermi level is equated to the Fermi level E_F in the grounded grain, since the difference between the two is only marginal. N_i (eV^{-1} m^{-2}) is the density of acceptor states in the GB. In our model, N_i is approximated by

$$N_i(E, \phi_b) = \begin{cases} \dfrac{Q_{i,max}}{e\,(\mu_2 - \mu_1)} & \text{if } \mu_1 + \phi_b \leq E \leq \mu_2 + \phi_b, \\ 0 & \text{else}, \end{cases} \quad (12)$$

where $Q_{i,max}$ (C m^{-2}) is the maximum charge in the GB due to the acceptor states, and μ_1 and μ_2 (eV) are the lower and upper limits of the rectangular distribution, respectively.

The integral of Eq. (10) was solved with the software Mathematica (Version 12.0, Wolfram Research, Inc., Champaign, IL, USA) and yielded,

$$Q_i = Q_{i,max}\left\{1 - \frac{k_B T}{\mu_2 - \mu_1}\left[\begin{array}{l} \ln\left(\exp\left(\dfrac{\mu_2 + \phi_b(Q_i)}{k_B T}\right) + \exp\left(\dfrac{E_F}{k_B T}\right)\right) \\ -\ln\left(\exp\left(\dfrac{\mu_1 + \phi_b(Q_i)}{k_B T}\right) + \exp\left(\dfrac{E_F}{k_B T}\right)\right) \end{array}\right]\right\}. \quad (13)$$

To calculate the current, first the barrier height ϕ_b must be calculated self-consistently by determining the charge Q_i from Eq. (13) for every value of applied voltage V. This was done with the root function of Mathematica (source code A in the supplementary material). When the voltage-dependent barrier height ϕ_b is known, it is easy to calculate the current J_{GB} from Eq. (9).

To account for the resistivity of the grain bulk, which is relevant for the high current region ($J > 1$ kA/cm^2), a serial resistance of $R = L/\sigma_{ZnO} = 1.4 \times 10^{-4}$ Ω (with grain diameter $L = 15$ μm and ZnO resistivity $\sigma_{ZnO} = 10.8$ S/cm) to the DSB was assumed, giving a total current J across the GB,

$$J(V) = \frac{V}{R + V_1/J_{GB}(V_1)}. \quad (14)$$

It must be mentioned that this formula is derived from some strong simplifications that are based on the BGM, which are: The GB and the piezo surface charges are homogenous and located at infinitely thin space regions, while the piezocharges are separated by a uniform dielectric with thickness d, the current is only caused by thermionic emission, and the donor densities are constant in the depletion regions of the grains. Also, influences of the inverse piezoelectric effect[31] are not included in the model to keep it simple.

TABLE I. Different models for the double Schottky barrier height ϕ_b (eV): (i) model of Blatter and Greuter, formula (6) in Ref. 3 (without deeper traps), the permittivities $\varepsilon_{1,2}$, and the donor densities $N_{1,2}$ of both grains are the same, symmetric with respect to the applied voltage V; (ii) model of Verghese and Clarke, formula (1) in Ref. 14 same as (i) but with a piezoelectric induced surface charge Q_p, symmetric with respect to V; (iii) model introduced in this work, for the case $\varepsilon_1 N_1 = \varepsilon_2 N_2$ with different surface charges Q_{p1} and Q_{p2} and an electric dipole moment $p_i = d(Q_{p1} - Q_{p2})$ at the GB, asymmetric with respect to V if $p_i < 0$ (p_i is defined negative or zero); (iv) model introduced in this work, for the case $\varepsilon_1 N_1 \neq \varepsilon_2 N_2$, the plus sign in front of the square root has to be applied for $\varepsilon_1 N_1 > \varepsilon_2 N_2$ and the minus sign for $\varepsilon_1 N_1 < \varepsilon_2 N_2$, always asymmetric with respect to V. e is the elementary charge, $N_{1,2}$ (m^{-3}) is the donor density of left, right grain, $\varepsilon_{1,2}$ is the permittivity of left, right grain, Q_i ($C\,m^{-2}$) is the interface charge due to trap states, $Q_{p1,2}$ ($C\,m^{-2}$) is the piezo- or polarization charge of left, right grain, V is the applied voltage, $p_i = d\,(Q_{p1} - Q_{p2})$ ($C\,m^{-1}$) is the electric dipole at interface, d is the interface thickness, and ε_i is the permittivity of interface.

$\varepsilon_1 N_1 = \varepsilon_2 N_2 = \varepsilon N$	Symmetric	(i) $\phi_b = \frac{(Q_i^2 - 2e\varepsilon NV)^2}{8\varepsilon N Q_i^2}$ $V \geq 0$.
		(ii) $\phi_b = \frac{((Q_i + Q_p)^2 - 2e\varepsilon NV)^2}{8\varepsilon N (Q_i + Q_p)^2}$ $V \geq 0$.
	Asymmetric	(iii) $\phi_b = \begin{cases} eV + \frac{((Q_i + Q_{p1} + Q_{p2})^2 - 2e\varepsilon N(V + p_i/\varepsilon_i))^2}{8\varepsilon N (Q_i + Q_{p1} + Q_{p2})^2} & \text{if } V \leq 0, \\ \frac{((Q_i + Q_{p1} + Q_{p2})^2 - 2e\varepsilon N(V + p_i/\varepsilon_i))^2}{8\varepsilon N (Q_i + Q_{p1} + Q_{p2})^2} & \text{if } V \geq 0. \end{cases}$
$\varepsilon_1 N_1 \neq \varepsilon_2 N_2$	Asymmetric	(iv) $\phi_b = \begin{cases} eV + \frac{e^2 N_1}{2\varepsilon_1} \left\{ \frac{\varepsilon_1 (Q_i + Q_{p1} + Q_{p2})}{e\,(\varepsilon_1 N_1 - \varepsilon_2 N_2)} \pm \sqrt{\frac{N_2}{N_1} \frac{\varepsilon_1 \varepsilon_2}{e\,(\varepsilon_1 N_1 - \varepsilon_2 N_2)} \left[\frac{(Q_i + Q_{p1} + Q_{p2})^2}{e\,(\varepsilon_1 N_1 - \varepsilon_2 N_2)} + 2V + 2\frac{p_i}{\varepsilon_i} \right]} \right\}^2 & \text{if } V \leq 0, \\ \frac{e^2 N_1}{2\varepsilon_1} \left\{ \frac{\varepsilon_1 (Q_i + Q_{p1} + Q_{p2})}{e\,(\varepsilon_1 N_1 - \varepsilon_2 N_2)} \pm \sqrt{\frac{N_2}{N_1} \frac{\varepsilon_1 \varepsilon_2}{e\,(\varepsilon_1 N_1 - \varepsilon_2 N_2)} \left[\frac{(Q_i + Q_{p1} + Q_{p2})^2}{e\,(\varepsilon_1 N_1 - \varepsilon_2 N_2)} + 2V + 2\frac{p_i}{\varepsilon_i} \right]} \right\}^2 & \text{if } V \leq 0. \end{cases}$

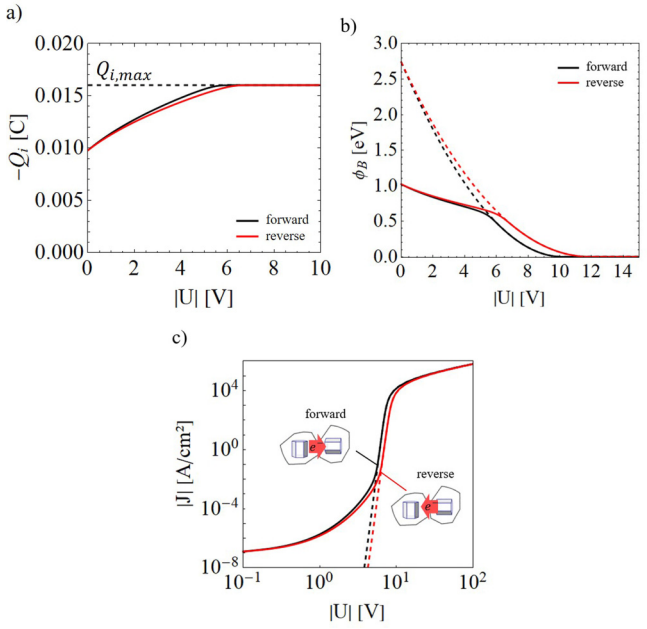

FIG. 3. Electric characteristic of a grain boundary formed by two grains with different orientations. The direction-dependent permittivity of the grains leads to asymmetric I–V behavior. (a) Interface charge Q_i self-consistently solved by Eq. (11); (b) double Schottky barrier height ϕ_b solved by Eq. (A9); (c) the current density J across the GB according to Eq. (12); dashed lines show the results for a constant interface charge $Q_i = Q_{i,max}$. However, the degree of I–V asymmetry depends strongly on the assumed density of acceptor states at the grain boundary.

III. RESULTS

A. Influence of different grain orientations

In a first study, the influence of different grain orientations on the I–V behavior was investigated (Fig. 3). When two grains with different orientations form a GB, asymmetric I–V behavior is expected with respect to the forward and reverse currents due to the direction-dependent permittivity of ZnO. For such a case, the DSB is described by Eq. (8). The parameters of the simulation (source code A in the supplementary material) are shown in Table II. The interface charge Q_i was solved self-consistently by Eq. (13). The result is depicted in Fig. 3(a) (solid lines). The negative interface charge increases with applied voltage as the number of occupied electron states at the GB increases and reaches a maximum when all interface states are occupied. Interestingly, this increase is slightly different for forward and reverse bias, which is a consequence of the fact that $\varepsilon_1 N_1 \neq \varepsilon_2 N_2$.

The forward–reverse asymmetry is also evident for the barrier height, which is calculated by Eq. (8) using the self-consistently solved charge Q_i [solid lines in Fig. 3(b)]. The dashed lines show how the DSB would behave if Q_i would not be dependent on the applied voltage but constant $Q_i = Q_{i,max}$. Even in this case, the barrier height exhibits asymmetric behavior because $\varepsilon_1 N_1 \neq \varepsilon_2 N_2$. Figure 3(c) shows the current across the DSB, calculated by Eq. (14) with the voltage-dependent barrier ϕ_b of Fig. 3(b). The small hexagons in Fig. 3(c) illustrate the different grain orientations (hexagonal Wurtzit structure). The pre-breakdown current in the forward direction (electrons moving from the mantle-side into the head or tail-side of the ZnO crystal/grain) is a little higher, and the switching voltage is a little lower.

The reason for this asymmetry lies solely in the different permittivities ε_1 and ε_2 of the grains. It must be mentioned that this kind of forward–reverse asymmetry of the pre-breakdown current is

TABLE II. Parameters of the simulations: ε_1 and ε_2 are the permittivities of grains 1 and 2, respectively; ε_0 is the permittivity of the vacuum; N_1 and N_2 are the donor densities of grains 1 and 2, respectively; d is the grain boundary width; $Q_{i,max}$ is the maximum interface charge due to electron acceptor states in the grain boundary; μ_1 and μ_2 are lower and upper limits of the rectangular density of (acceptor) states, respectively; Q_{p1} and Q_{p2} are the piezoelectric and/or polarization surface charges; other parameters: $T = 400$ K, $E_F = 3.2$ eV, $A^* = 30$ A cm^{-2} K^{-2}, $\varepsilon_\xi = 0.067$ eV, and $\varepsilon_i = 2/(1/\varepsilon_1 + 1/\varepsilon_2)$.

	Figure 3	Figure 4	Figure 5	Figure 6
ε_1 [ε_0]	7.6	7.6	7.6	8
ε_2 [ε_0]	8.9	8.9	8.5	8
N_1 (m^{-3})	10^{24}	10^{24}	1.3×10^{23}	10^{24}
N_2 (m^{-3})	10^{24}	10^{24}	2×10^{23}	(a) 10^{24} (b) 3×10^{23}
d (m)	10^{-9}	10^{-9}	45×10^{-9}	0
$Q_{i,max}$ (C m^{-2})	−0.0162	−0.0162	−0.0104	(a) −0.0213 (b) −0.0192
μ_1 (eV)	1.5	1.5	2.3	(a) 1.5 (b) 2.55
μ_2 (eV)	2.5	2.5	3.1	(a) 3.2 (b) 2.85
Q_{p1} (C m^{-2})	0	(a) 0 (b) 0 (c) 0 (d) 0	0 0	0
Q_{p2} (C m^{-2})	0	(a) 0 (b)1.17×10^{-4} (c)5.84×10^{-4} (d)1.17×10^{-3}	(a) 0 (b) -2.63×10^{-2}	0

strongly dependent on the density of states at the interface. Here, a rectangular density of states, as defined in Eq. (12), with an energy width of $\mu_2 - \mu_1 = 1$ eV was adopted. The greater this width is, the greater the forward–reverse asymmetry. Other simulations (not shown here) with narrower densities of states of $\mu_2 - \mu_1 < 0.1$ eV lead to nearly symmetric I–V behavior in the pre-breakdown region.

Moreover, this study—like all others in this article—must be considered as a particular, idealized case used only to provide an understanding of the factors responsible for the asymmetry of the forward and reverse currents. Real grain boundaries are not formed by perfectly smooth crystal planes. They have a certain curvature, roughness, and the interfacial layer is not uniform in thickness. Since the product of donor density and dielectric constant is crucial (and not ε alone) even for artificial grain boundaries of bicrystals with well-defined orientations and contact faces there remains an uncertain, possibly spatially distributed donor profile.

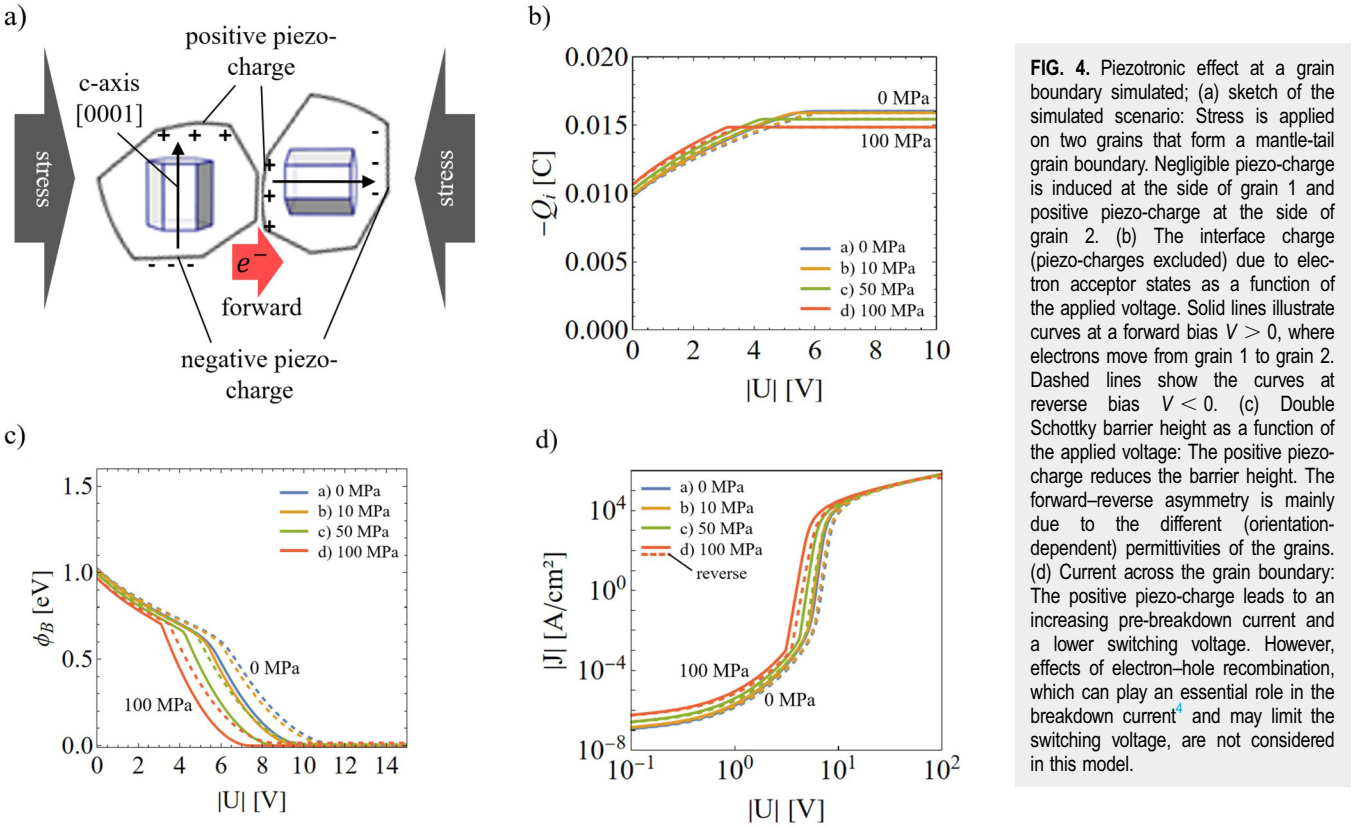

FIG. 4. Piezotronic effect at a grain boundary simulated; (a) sketch of the simulated scenario: Stress is applied on two grains that form a mantle-tail grain boundary. Negligible piezo-charge is induced at the side of grain 1 and positive piezo-charge at the side of grain 2. (b) The interface charge (piezo-charges excluded) due to electron acceptor states as a function of the applied voltage. Solid lines illustrate curves at a forward bias $V > 0$, where electrons move from grain 1 to grain 2. Dashed lines show the curves at reverse bias $V < 0$. (c) Double Schottky barrier height as a function of the applied voltage: The positive piezo-charge reduces the barrier height. The forward–reverse asymmetry is mainly due to the different (orientation-dependent) permittivities of the grains. (d) Current across the grain boundary: The positive piezo-charge leads to an increasing pre-breakdown current and a lower switching voltage. However, effects of electron–hole recombination, which can play an essential role in the breakdown current[4] and may limit the switching voltage, are not considered in this model.

Another important point is that the switching voltage can strongly vary according to the presented approach. Switching voltages of 20 V and higher were simulated (not shown here). To the authors' knowledge, such high switching voltages were never observed for ZnO DSBs. Grain–grain I–V measurements on ZnO varistors typically exhibit switching voltages in the range of 3–4.5 V.[32] Blatter and Greuter explained the switching voltage as caused by electron–hole generation and recombination.[4] Effects of electron–hole recombination were not considered in the present model so that the breakdown current is not described correctly. Only the pre-breakdown current can be accurately described within the scope of this model.

B. Influence of piezoelectric charges—Piezotronic effect

The influence of piezoelectric surface charges on the GB behavior was simulated. The GB was assumed to be formed by two grains with mantle-tail orientation [Fig. 4(a)]. A stress T_3 of 0, −10, −50, and −100 MPa is applied perpendicular to the GB. (T_3 is negative for compressive stress.) The left grain in Fig. 4(a) is grain 1 with negligible piezoelectric surface charge ($Q_{p1} = 0$) at the GB. The right grain contributes a piezocharge $Q_{p2} = -d_{p,33} T_3$ to the GB (listed in Table II), with $d_{p,33} = 11.67 \times 10^{-12}$ C/m^2 being the piezoelectric stress coefficient of ZnO along to the c axis (value taken from Ref. 33, p. 445). The piezoelectric induced charge Q_{p2} influences the barrier height ϕ_b [Eq. (8)], which influences the interface charge Q_i [Eq. (13)] as illustrated in Fig. 4(b). The solid lines show the result at forward bias ($V > 0$) and the dashed lines at reverse bias ($V < 0$). At high voltage, the self-consistently solved Eq. (13) yielded that less interface states can be occupied the higher the stress (the larger the positive piezo-charge). At low voltages, more interface states are occupied for positive Q_{p2}, leading to more interface charge Q_i. This effect of an increase in interface charge counteracts the reduction of the barrier by the positive piezo-charge, but still leads to a reduction of the barrier as shown in Fig. 4(c). The forward–reverse asymmetry is mainly due to the different permittivities of the grains (different grain orientations). In the particular case simulated here, the piezo-charge contributes only marginally to this asymmetry but causes a significant increase in pre-breakdown current [Fig. 4(d)]. This result matches very well with the results published by Keil *et al.*[28] and confirms the experimental observation of increasing current when positive piezo-charge is induced at the GB.[19,21] According to the simulations, the switching voltage is shifted, as was also found by Keil *et al.*[18]

However, as already explained, the breakdown current is not correctly described by the model presented. Such drastic shifts of the switching voltages are not observed for real GBs as demonstrated by Billovits *et al.*[21] They published I–V measurements on individual GBs under uniaxial stress. Four of these measurements are depicted in Fig. 5 (the same as shown by Billovits *et al.*, Fig. 4 in Ref. 21). The forward and reverse curves with no applied stress are colored black, and the curves with an uniaxial strain of 5×10^{-4} are colored red. Symbols illustrate the measurement and solid lines the simulated curves. An electron backscatter diffraction image (EBSD) of the grains is shown in the inset 1 of Fig. 5, with the grain orientations and the forward current (movement of the electrons) shown. Billovits *et al.* calculated the induced piezoelectric charge on the GB due to the uniaxial strain to be 2.625×10^{-4} C/m^2 for the larger, tail-oriented grain and to be -0.030×10^{-4} C/m^2 for the smaller, nearly mantle-oriented grain. These values were incorporated into the simulation where the other parameters were adjusted to the non-stressed I–V curves.

The GB showed an asymmetric forward–reverse I–V behavior (with and without applied stress), which could not be explained by the different grain orientations alone. It was also necessary to assume a difference in donor densities by a factor of $N_1/N_2 = 0.65$. In this way, it was possible to reproduce the measured pre-breakdown current in forward and reverse direction with good accuracy, with and without induced piezo-charge. A very interesting observation of the measured I–V curves of Billovits *et al.* was the fact that only the forward pre-breakdown current increased when stress was applied on the grains. The reverse current showed no significant response on the stress. The cause of this strange asymmetric piezotronic effect was completely unclear, but can be explained by the present model under the assumption that the GB is $d \approx 45$ nm wide. Simulation tests (not shown here) revealed that

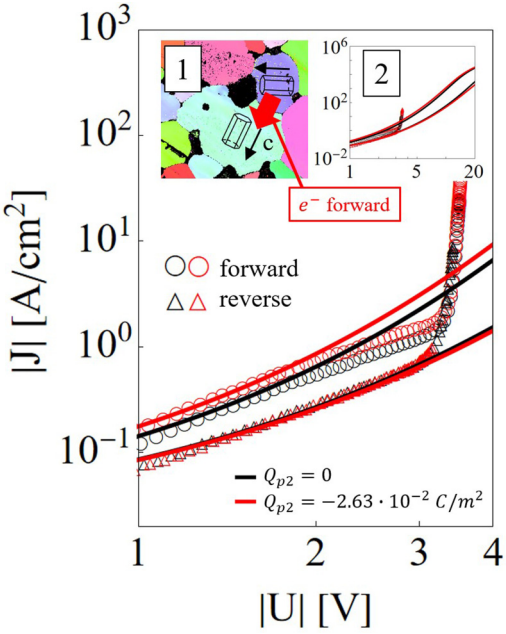

FIG. 5. Piezotronic modification of a ZnO grain boundary: Measured I–V data (circular and triangular symbols) of a single grain boundary (taken from Billovits *et al.*,[21] Fig. 4 in their paper) without applied stress (black symbols and curves) and with applied stress (red). The I–V behavior shows forward–reverse asymmetry due to the different grain orientations and probably due to different donor densities. Inset 1 shows an EBSD image with the orientations of the two involved grains. Under applied external stress, a piezo-charge Q_{p2} is induced at the side of the larger grain (green in inset 1), leading to an increase in pre-breakdown current. Solid lines show the results of the simulations with the parameters listed in Table II. The pre-breakdown current can be described quite well. At a voltage >3.5 V, there is a significant discrepancy between the model and the measurement (inset 2, same units). This is probably due to the effects of electron–hole generation,[4] which causes a sharp increase in current (breakdown) and which is not accounted for in the present model.

the GB thickness influences the increase in pre-breakdown current, whereas a wider GB can cause asymmetric change in pre-breakdown current and can even lead to an increase in one current direction and a decrease in the other current direction. The discrepancy between experiment and simulation, especially for the forward currents, could be due to the interface density of states, which, on the one hand, may not be sufficiently well modeled by a rectangular distribution or may even need to be considered as spatially distributed over 45 nm (which is quite large). Another important point is, as shown in inset 2 of Fig. 5, that the current at a voltage >3.5 V is significantly underestimated by the model. As mentioned before, this is probably due to the effects of electron–hole generation,[4] which causes a sharp increase in current (breakdown) and which are not accounted for in the present model. However, the pre-breakdown current can be described impressively accurate.

C. Degradation of a DSB

The high or long-term applied voltage can alter the I–V curves of varistors, leading to higher leakage currents (at DC) or power losses (at AC).[34] This aging phenomenon is called degradation and has been described in the literature for more than 40 years, but its cause has been the subject of debate for some time.[29] In their review article of 2016, He *et al.*[29] attempt to draw a line and concluded that the degradation of ZnO DSBs is caused by ion migration of Zn-interstitials.

Interestingly, varistor degradation after a prolonged or high-impulse DC current can cause an asymmetric shift in the I–V curve,[34] the reverse current increases more than the forward current (after a forward bias), which could be demonstrated also for individual GBs by Wang *et al.*[25] Although this effect has been qualitatively explained in the 1970s–1990s by Eda,[35] Hayashi *et al.*,[36] and Greuter[37] to be caused by asymmetric net donor profiles in the space charge regions and experimentally supported by a work of Cheng *et al.*[38] who showed that the ion migration at ZnO GBs is correlated with charge displacement, leading to a less negative charge in the GB and a less positive charge at the side of the long-term positively biased grain, a fully comprehensive model is still missing.

Implementing the result of Cheng *et al.*[38] into our model by assuming less interfacial charge $Q_{i,max}$ (less negative charge in the GB), less donors N_2 at grain 2 (less positive charge there), and a smaller energy width of the density of acceptor states (defined by μ_1 and μ_2) for the degraded GB (values shown in Table II), it is possible to describe the observed asymmetric I–V curves from Wang *et al.*[25] (Fig. 6) supporting the phenomenological explanations of Eda,[35] Hayashi *et al*,[36] and Greuter.[34,37] The third assumption concerning the energy width of the density of states was necessary to explain the weaker nonlinear I–V behavior of the degraded GB. Simulation tests showed that the energy width of the density of states has a distinct effect on the nonlinear behavior of the pre-breakdown current. The wider this width is, the higher the nonlinearity. Assuming a narrower energy width after degradation means that some of the acceptor states in the GB are no longer present. The presented model can explain the observations of Wang *et al.*[25] very well: the increase in pre-breakdown current, the forward–reverse asymmetry, and even the less nonlinear behavior after degradation. Thus, the present model also provides an explanation of how there can be a larger increase in leakage current from varistors in the reverse direction after a prolonged forward current, in agreement with the degradation explanations of He *et al*,[29] Eda,[35] Hayashi *et al*,[36] and Greuter[34,37] The narrower energy width of the acceptor states in the GB after degradation, however, should be taken with some caution. Previous studies have shown that the energy level of the interfacial states is quite constant in all the varistor materials studied.[34] On the other hand, these studies did not treat highly degraded GBs.

D. Influence of surface polarity and wide, conductive grain boundaries

To the authors' knowledge, the work of Cheng *et al.*[27] was the first to provide an explanation of the asymmetric I–V behavior of DSBs. In their paper, "artificial" DSBs of ZnO bicrystals with defined crystal orientations were studied. They found highly asymmetric I–V behavior (Fig. 7) for crystal orientations with different surface polarities (O and Zn-polar faces forming the DSB), and explained this behavior in terms of asymmetric DSBs, concluding that O-faces lead to lower Schottky barriers than Zn-faces. The reason given for this is different surface charges on either side because of the spontaneous polarization of ZnO and possible ion migration processes during sintering. In their paper, the current across the DSB is described by Eq. (9). Their simulated results for forward and reverse currents are shown as dashed lines in Fig. 7.

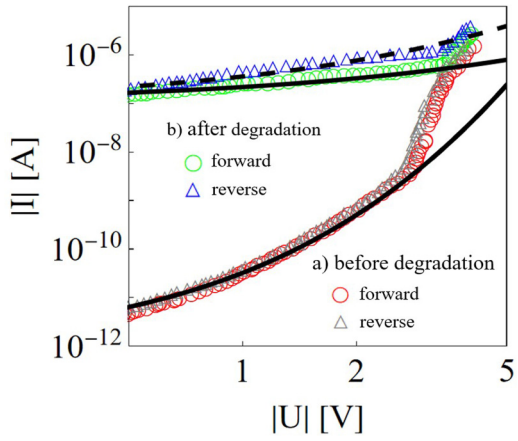

FIG. 6. Applying the present model to the measured I–V data from a degraded grain boundary published by Wang *et al.*,[25] Fig. 6 in their paper The forward and reverse curves before degradation (curves a) are nearly identical. Applying 5.7 V for 15 h with an approximate forward current of 40 μA under a temperature of 100 °C leads to a strong increase in pre-breakdown current (curves b) with a slight forward–reverse asymmetry. The simulated curves are represented by the solid (forward) and dashed (reverse) lines. The increase in pre-breakdown current is caused by less negative charge in the grain boundary after degradation. The forward–reverse asymmetry after degradation can be explained by fewer donors in the depletion region of grain 2 (the positively charged grain at the forward current). The lower nonlinear I–V behavior after degradation is due to a narrower energy width of the density of acceptor states in the grain boundary.

All attempts to reproduce the measurement curves of Cheng *et al.*,[27] shown in Fig. 7, with the previously presented model did not yield satisfactory results, probably because the GB is too wide, with a thickness of 25 μm, and because it is an ohmic conductor. The presented model should only be applied on very thin GBs. For conductive GBs thicker than ~100 nm, DSB should be better treated as two back-to-back connected Schottky diodes. Actually, the work of Cheng *et al.* uses a similar approach. They apply Eq. (9) with a constant Schottky barrier height in contrast to the approach of Blatter and Greuter who assume a voltage-dependent barrier height (and interface charge). However, Cheng *et al.* do not consider the reverse-biased barrier, which is a significant shortcoming of their approach. In our model, presented below, the DSB is treated as two back-to-back connected Schottky diodes where the reverse-biased barrier is also taken into account.

The forward current across Schottky barriers of ZnO–Pd and ZnO–Ag Schottky contacts in varistors have been recently investigated and described by[39,40]

$$J_+ = A^* T^2 \exp\left(-\frac{\phi_{SB}}{k_B T}\right)\left[\exp\left(\frac{e\,V}{n k_B T}\right) - 1\right] \quad \text{for } (V > 0), \tag{15}$$

and the reverse current can be described by[40]

$$J_- = A^* T^2 \exp\left(-\frac{\phi_0 - \Delta\phi}{k_B T}\right)\left[\exp\left(\frac{e\,V}{n k_B T}\right) - 1\right] + 1\ \text{A/cm}^2 \left(\frac{|V|}{V_b}\right)^{\alpha} \quad \text{for } (V < 0), \tag{16}$$

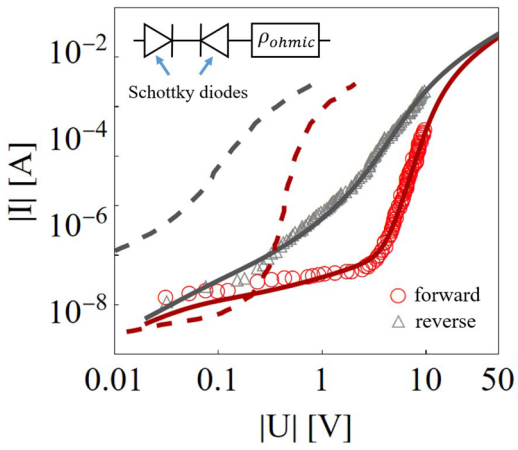

FIG. 7. Measured I–V data (circular and rectangular symbols) across a bicrystal grain boundary formed by two crystals with O and Zn-polar faces, published by Cheng *et al.*,[27] Fig. 1(d) in their paper. At forward current, the Zn-polar (0001) face is positively biased (i.e., the O-polar face is the forward biased Schottky barrier and the Zn-polar face is the reverse-biased Schottky barrier). The solid lines show the simulated results of the present model. The dashed lines show the simulated results of Cheng *et al.*[27] Red curves represent forward current and grey curves reverse current.

with n the ideality factor, ϕ_{SB} the effective Schottky barrier height at $V = 0$, ϕ_0 the undiminished Schottky barrier height at $V = 0$, diminished by the reverse current correction,

$$\Delta\phi = e(\Delta\varphi_{image} + c\mathscr{E}), \tag{17}$$

with the image force lowering,

$$\Delta\varphi_{image} = \sqrt{\frac{e\,\mathscr{E}}{4\pi\ \varepsilon_{1,2}}}, \tag{18}$$

and a term $ec\mathscr{E}$ where c is a voltage-independent constant in units of length and $\mathscr{E}$ is the electric field strength at the ZnO–metal interface, in the depletion approximation given by

$$\mathscr{E} = \sqrt{\frac{2\,e\,N_{1,2}(\phi_0/e - V_n - V)}{4\pi\,\varepsilon_{1,2}}} \quad (V < 0). \tag{19}$$

Here, V_n is the difference between the Fermi level and the conduction band minimum in the grain.

The second summand in Eq. (16) accounts for the breakdown current, which is associated with electron–hole generation and annihilation processes, whereas V_b is the breakdown voltage, here defined as the voltage when the breakdown current equals 1 A/cm^2. α is the nonlinear coefficient of the breakdown current.

The measured I–V data from Cheng *et al.*[27] can be described very well by connecting a forward and a reverse Schottky diode, described by Eqs. (15) and (16), in series with an ohmic resistance (resistance times area),

$$\rho_{ohmic} = \rho_{\mathrm{ZnO}}\, l + \rho_{gb}\, d, \tag{20}$$

where ρ_{ZnO} (resistance times length) is the resistivity of the grain bulk, l is the distance the current flows through the grain bulk, ρ_{gb} (resistance times length) is the resistivity of the interfacial layer, and d is its thickness.

The current through the two back-to-back Schottky diodes connected serially with the resistance ρ_{ohmic} can be solved numerically as demonstrated in a previous publication.[41] The program code is shown in the supplementary material. The results of the simulations are plotted in Fig. 7. The simulation parameters were fitted manually to the measured curves. It can be seen that the measurement results can be reproduced very well, significantly better than with the simulations of Cheng *et al.* The fitted parameters were: $\phi_{SB} = 0.79$ eV, $n = 1$, $\phi_0 = 0.84$ eV, $N_{1,2} = 10^{23}$ m^{-3}, $V_n = 0.5$ V, $V_b = 33$ V, and $\alpha = 7$. The predefined assumed parameters were: $\varepsilon_{1,2} = 8\,\varepsilon_0$, $\rho_{ZnO} = 10\ \Omega$ cm, $\rho_{gb} = 10^6\ \Omega$ cm, $l = 1$ mm, and $d = 25\,\mu$m. The high breakdown voltage $V_b = 33$ V, which for metal/ZnO contacts is typically 2.5–3.5 V,[40] should not be too irritating since it is defined here as the voltage at which the breakdown current is 1 A/cm^2, not the voltage at which breakdown actually occurs.

The low nonlinear coefficient $\alpha = 7$ (low compared to the α in commercial varistors[40]) leads to such high V_b. Interestingly, all of the simulation parameters are identical for the O and the

Zn-polar face. There was only one parameter that was different and that is the voltage-independent constant c from Eq. (17), which is $c = 3$ nm for the Zn-polar side and $c = 0$ for the O-polar side. c lowers the barrier and enhances the reverse current. It can be interpreted as an effect due to an additional interfacial layer as was discussed in a previous work[39] and in Sec. 1.4.3, Eqs. (1.17) and (1.18) of Ref. 42. Thus, according to this model, the only difference between the O-polar and the Zn-polar face is that there is an additional (probably dielectric or highly resistive) layer at the Zn-polar face, which is not present at the O-polar side. This layer is presumably formed during sintering because of the influence of the spontaneous polarization of the ZnO.

IV. SUMMARY AND DISCUSSION

We provide a model that can describe the I–V behavior (at least in the pre-breakdown region) of asymmetric and piezotronically modified double Schottky barriers (DSBs) at ZnO grain boundaries (GBs). The model is based on an extension and generalization of the GB model of Blatter and Greuter,[3] where the influence of different grain orientations (different permittivities), different donor densities, piezoelectric charges, and a possible electric dipole moment are incorporated. It was found that the product of permittivity and donor density is crucial. If this product is equal for both grains that form the GB, and if there is no electric dipole and no piezoelectric charge at the GB, the presented model is equal to the model of Blatter and Greuter[3] or its extension to interfacial piezocharges as modeled by Verghese and Clarke.[14] If the product of permittivity and donor density differs, the GB I–V behavior is asymmetric (forward and reverse currents differ to some degree). Thus, GBs with differently oriented grains should show asymmetric I–V behavior (if this effect is not compensated by the donor densities). The resulting asymmetry, however, is weak (Fig. 3). Furthermore, the model confirms that piezoelectrically induced charges at the GB can increase and decrease the pre-breakdown current. These charges can also cause an electric dipole that leads to forward–reverse asymmetry (Fig. 4). This was also confirmed by measurements[21] (Fig. 5). The question of whether the current increases or decreases in forward and reverse direction and to what extent cannot be answered in general terms, since the charge in the GB, and, therefore, the barrier height, is dependent on the density of acceptor states and the GB width. The problem must be solved self-consistently.

Furthermore, the model can explain the increase in current and the forward–reverse asymmetry of degraded GBs (Fig. 6), in good agreement with the explanation of DSB degradation by He *et al.*,[29] Eda,[35] Hayashi *et al*,[36] and Greuter.[34,37] According to our results, the increase in current for degraded GBs is due to a lower interfacial charge, whereas the asymmetry is caused by fewer electron donors in the depletion region of the long-term positively biased grain. Although there is good agreement between our model and the pre-breakdown I–V measurements of individual GBs (Figs. 5 and 6), these results should not be overestimated. Current measurements on GBs are still challenging and can be influenced and distorted by many factors like the sample preparation, surroundings [temperature, light sources (especially UV light), oxygen partial pressure, etc.], measurement time, and the current and power densities of the measurement. In particular, the pre-breakdown current, which is described by our model, is often affected. Mechanical polishing to access individual GBs results in electronic defects that can significantly influence the measured currents.[43] Also, I–V measurements on GBs usually reach high current (>10 A/cm^2) and power densities (>30 W/cm^2), which can change the I–V curves temporarily (due to heat or degradation) or permanently (due to degradation).[34] In addition, the currents across a single GB in the region before breakdown are usually very small (in the range of 1–100 nA or even smaller), so that capacitance effects of the measuring equipment or the GB itself can significantly influence the result. These capacitance effects require a measurement duration in the low current range that is not too short, while heating effects and possible degradation require a measurement duration in the high current range that is not too long. These issues are often not considered.

Moreover, two shortcomings of the model must be mentioned: First, it cannot describe the current in the breakdown region correctly. Arguably, the effects of electron–hole generation and recombination must also be taken into account for the breakdown current.[4] Second, the model fails to describe sandwich-like bicrystals as studied by Cheng *et al.*[27] (Fig. 7). However, it could be demonstrated in Sec. III D that such DSBs can be described by a previously published model,[40,41] when the DSB is treated as an ohmic layer and the layer/ZnO junctions are treated as two back-to-back Schottky contacts. With such an approach, the measured I–V data of Cheng *et al.*[27] could be reproduced very well. Cheng *et al.* explained the forward–reverse asymmetry by different Schottky barrier heights for O and Zn-polar faces. Our results, however, suggest that the barrier heights do not differ significantly, in agreement with previously found results,[39] where it was observed that the height of the Schottky barrier of grain-to-electrode interfaces in ZnO varistors does not depend on the grain orientation. According to our simulations, the asymmetry found by Cheng *et al.* can solely be explained by an additional, very thin (a few nanometers), probably dielectric or highly resistive interfacial layer at the Zn-polar surface. One possible explanation is that this layer at the Zn-polar face is formed during sintering, possibly triggered by the spontaneous polarization of ZnO. However, the artificial DSB of Cheng *et al.*[27] should be compared with GBs in bulk material only with caution. Whether there is any dependence of the natural polarity of ZnO on the formation of the GB and the DSB (e.g., through the donor profile) remains an open question.

An interesting question is how the first model, which treats thin (<100 nm) "natural GBs" that are common in varistors, transitions to the second model, which treats wide or "artificial GBs," called "sandwich-like structures," where the interfacial layer is distinctly thicker. In fact, the models do not converge. They represent two different approaches to two different problems. In the first case, the electrostatic barrier responsible for blocking the current flow is caused by a negative interface charge that is located in a narrow region compared to the depletion regions in the grains. In the second case, where the interfacial layer is wide compared to the depletion regions, there are two spatially separated barriers, one on each side of the interfacial layer. The crucial difference between these two approaches is that in the second case, there is a

conductive layer that screens one side (i.e., one barrier) from the other. In the first case, there is no such screening and the barrier can be considered as caused by a uniformly distributed charge in the GB. Where this charge is actually located is not important for the model as long as the electric field caused by the charge (as perceived in the depletion regions of the grains) can be accurately described by the Dirac delta distribution given in Eq. (3).

SUPPLEMENTARY MATERIAL

In the supplementary material, two program codes, source codes A and B (Mathematica, Version 12.0, Wolfram Research, Inc., Champaign, IL, USA), are available online as a PDF document. Source code A contains the calculation to Sec. III A and shows the curves of Fig. 3. It is the basis for all calculations of the model used in Secs. III A–III C. Source code B provides the program code to the model presented in Sec. III D showing the calculated curves of Fig. 7.

ACKNOWLEDGMENTS

The authors gratefully acknowledge financial support under the scope of the COMET program within the K2 Center "Integrated Computational Material, Process and Product Engineering (IC-MPPE)" (Project No. 859480). This program was supported by the Austrian Federal Ministries for Transport, Innovation and Technology (BMVIT) and for Digital and Economic Affairs (BMDW), represented by the Austrian research funding association (FFG), and the federal states of Styria, Upper Austria and Tyrol.

AUTHOR DECLARATIONS

Conflict of Interest

The authors have no conflicts to disclose.

Author Contributions

Benjamin Kaufmann: Conceptualization (lead); Data curation (lead); Formal analysis (lead); Investigation (lead); Methodology (lead); Software (lead); Visualization (lead); Writing – original draft (lead); Writing – review & editing (lead). **Peter Supancic:** Formal analysis (supporting); Funding acquisition (lead); Investigation (supporting); Methodology (supporting); Project administration (lead); Software (supporting); Supervision (lead); Validation (lead); Visualization (supporting); Writing – original draft (supporting); Writing – review & editing (supporting).

DATA AVAILABILITY

The data that support the findings of this study are available from the corresponding author upon reasonable request.

APPENDIX: DERIVATION OF THE DSB HEIGHT

To determine the barrier height at the GB, Eq. (6) must be solved for the two unknowns x_1 and x_2. This gives us a solution for the electric potential $\varphi(x)$, which is discontinuous at $x = 0$ if $p_i \neq 0$. x_1 and x_2 are determined by the conditions of charge neutrality,

$$e(-N_1 x_1 + N_2 x_2) + Q_i + Q_{p1} + Q_{p2} = 0, \tag{A1}$$

and the transition at $x = 0$, which is

$$\varphi(0^-) = \varphi(0^+) + p_i/\varepsilon_i. \tag{A2}$$

Solving Eqs. (A1) and (A2) for x_1 and x_2, we found the fairly simple solution for the case $\varepsilon_1 N_1 = \varepsilon_2 N_2$,

$$\begin{aligned} x_1 &= \frac{Q_i + Q_{p1} + Q_{p2}}{2eN_1} - \frac{\varepsilon_1 p_i}{\varepsilon_i (Q_i + Q_{p1} + Q_{p2})} - \frac{\varepsilon_1 V}{(Q_i + Q_{p1} + Q_{p2})}, \\ x_2 &= -\frac{Q_i + Q_{p1} + Q_{p2}}{2eN_1} - \frac{\varepsilon_1 p_i}{\varepsilon_i (Q_i + Q_{p1} + Q_{p2})} - \frac{\varepsilon_1 V}{(Q_i + Q_{p1} + Q_{p2})}, \end{aligned} \tag{A3}$$

and for the case $\varepsilon_1 N_1 \neq \varepsilon_2 N_2$, we found

$$\begin{aligned} x_1 &= \frac{\varepsilon_1 (Q_i + Q_{p1} + Q_{p2})}{e(\varepsilon_1 N_1 - \varepsilon_2 N_2)} \pm \sqrt{\frac{N_2}{N_1} \frac{\varepsilon_1 \varepsilon_2}{e(\varepsilon_1 N_1 - \varepsilon_2 N_2)} \left[\frac{(Q_i + Q_{p1} + Q_{p2})^2}{e(\varepsilon_1 N_1 - \varepsilon_2 N_2)} + 2V + 2\frac{p_i}{\varepsilon_i} \right]}, \\ x_2 &= d + \frac{\varepsilon_1 (Q_i + Q_{p1} + Q_{p2})}{e(\varepsilon_1 N_1 - \varepsilon_2 N_2)} \pm \sqrt{\frac{N_1}{N_2} \frac{\varepsilon_1 \varepsilon_2}{e(\varepsilon_1 N_1 - \varepsilon_2 N_2)} \left[\frac{(Q_i + Q_{p1} + Q_{p2})^2}{e(\varepsilon_1 N_1 - \varepsilon_2 N_2)} + 2V + 2\frac{p_i}{\varepsilon_i} \right]}, \end{aligned} \tag{A4}$$

where the plus sign in front of the square root has to be applied for $\varepsilon_1 N_1 > \varepsilon_2 N_2$ and the minus sign for $\varepsilon_1 N_1 < \varepsilon_2 N_2$. Equations (A3) and (A4) are only valid until a critical voltage V_{c1} or V_{c2} is reached, when x_1 or x_2 becomes zero. This is the case if

$$\begin{aligned} V_{c1} &= -\frac{p_i}{\varepsilon_i} + \frac{(Q_i + Q_{p1} + Q_{p2})^2}{2e\varepsilon_2 N_2}, \\ V_{c2} &= -\frac{p_i}{\varepsilon_i} - \frac{(Q_i + Q_{p1} + Q_{p2})^2}{2e\varepsilon_1 N_1}, \end{aligned} \tag{A5}$$

where $V_{c1} > 0$ and $V_{c2} < 0$. Reaching V_{c1} or V_{c2}, the potential barrier at the GB disappears. By taking into account that the electrons move from grain 1 to grain 2 if $V > 0$ and that they are moving from grain 2 to grain 1 if $V < 0$, Eq. (A5) shows a very interesting result with respect to current flow: the critical voltage, at which the barrier completely disappears, depends only on the permittivity and donor density of the grain *into which the electrons move*, but not on the permittivity and donor density of the grain the electrons come from.

The barrier height $\phi_b = -e\varphi_b$ can be easily calculated from Eq. (6) by setting $\varphi_b = \varphi(0^-)$ if $p_i \leq 0$ and $\varphi_b = \varphi(0^+)$ if $p_i \geq 0$. When $p_i = 0$, it applies $\varphi_b = \varphi(0^-) = \varphi(0^+)$. The height of the double Schottky barrier can be written as

$$\phi_b = \begin{cases} -e\dfrac{p_i}{\varepsilon_i} & \text{if } V \leq V_{c2}, \\ eV + \dfrac{e^2 N_1 x_1^2}{2\varepsilon_1} & \text{if } V_{c2} < V \leq 0, \\ \dfrac{e^2 N_1 x_1^2}{2\varepsilon_1} & \text{if } 0 < V \leq V_{c1}, \\ 0 & \text{if } V_{c1} < V \end{cases} \tag{A6}$$

for the case $p_i \leq 0$, and it is

$$\phi_b = \begin{cases} 0 & \text{if } V \leq V_{c2}, \\ \dfrac{e^2 N_2 x_2^2}{2\varepsilon_2} & \text{if } V_{c2} < V \leq 0, \\ -eV + \dfrac{e^2 N_2 x_2^2}{2\varepsilon_2} & \text{if } 0 < V \leq V_{c1}, \\ e\dfrac{p_i}{\varepsilon_i} & \text{if } V_{c1} < V \end{cases} \tag{A7}$$

for the case $p_i \geq 0$.

Since the coordinate system can be chosen arbitrarily, the problem can always be defined in such a way that $p_i \leq 0$. To compare the result of Eq. (A6) with the approach of Verghese and Clarke[14] as formulated by Baraki *et al*[16] [Eq. (1)], x_1 from Eq. (A3) is put into Eq. (A6), giving the DSB height for the case if $\varepsilon_1 N_1 = \varepsilon_2 N_2$ and $V_{c1} \leq V \leq V_{c2}$,

$$\phi_b = \begin{cases} eV + \dfrac{((Q_i + Q_{p1} + Q_{p2})^2 - 2e\varepsilon_1 N_1 (V + p_i/\varepsilon_i))^2}{8\varepsilon_1 N_1 (Q_i + Q_{p1} + Q_{p2})^2} & \text{if } V \leq 0, \\ \dfrac{((Q_i + Q_{p1} + Q_{p2})^2 - 2e\varepsilon_1 N_1 (V + p_i/\varepsilon_i))^2}{8\varepsilon_1 N_1 (Q_i + Q_{p1} + Q_{p2})^2} & \text{if } V \geq 0. \end{cases} \tag{A8}$$

If $V \leq V_{c1}$ or $V \geq V_{c2}$, it applies $\phi_b = 0$. Equation (A8) is the more general formulation of Eq. (1) considering an electric dipole moment $p_i \leq 0$ at the GB. It is also possible to define ϕ_b with the assumption $p_i \geq 0$. This would result in a physically equivalent expression, but different signs in the formula. For reasons of clarity and simplicity only the case $p_i \leq 0$ is treated here. If $p_i = 0$, Eq. (A8) equals Eq. (1) for $V \geq 0$ and $V < 0$. The second case may not be obvious at first hand, but it can be easily checked by multiplying out both cases. If $p_i \neq 0$, the barrier height is asymmetric with respect to the applied voltage V. From this, it is evident that an electric dipole at the GB can cause asymmetric I–V behavior, as will be discussed in more detail below.

For the case $\varepsilon_1 N_1 \neq \varepsilon_2 N_2$ and $p_i \leq 0$, the DSB height can be determined by putting x_1 from Eq. (A4) into Eq. (A6), which yields for $V_{c1} \leq V \leq V_{c2}$,

$$\phi_b = \begin{cases} eV + \dfrac{e^2 N_1}{2\,\varepsilon_1} \left\{ \dfrac{\varepsilon_1 (Q_i + Q_{p1} + Q_{p2})}{e\,(\varepsilon_1 N_1 - \varepsilon_2 N_2)} \pm \sqrt{\dfrac{N_2}{N_1} \dfrac{\varepsilon_1 \varepsilon_2}{e\,(\varepsilon_1 N_1 - \varepsilon_2 N_2)} \left[\dfrac{(Q_i + Q_{p1} + Q_{p2})^2}{e\,(\varepsilon_1 N_1 - \varepsilon_2 N_2)} + 2V + 2\dfrac{p_i}{\varepsilon_i} \right]} \right\}^2 & \text{if } V \leq 0, \\ \dfrac{e^2 N_1}{2\,\varepsilon_1} \left\{ \dfrac{\varepsilon_1 (Q_i + Q_{p1} + Q_{p2})}{e\,(\varepsilon_1 N_1 - \varepsilon_2 N_2)} \pm \sqrt{\dfrac{N_2}{N_1} \dfrac{\varepsilon_1 \varepsilon_2}{e\,(\varepsilon_1 N_1 - \varepsilon_2 N_2)} \left[\dfrac{(Q_i + Q_{p1} + Q_{p2})^2}{e\,(\varepsilon_1 N_1 - \varepsilon_2 N_2)} + 2V + 2\dfrac{p_i}{\varepsilon_i} \right]} \right\}^2 & \text{if } V \geq 0. \end{cases} \tag{A9}$$

Again, the plus sign in front of the square root has to be applied for $\varepsilon_1 N_1 > \varepsilon_2 N_2$ and the minus sign for $\varepsilon_1 N_1 < \varepsilon_2 N_2$, and $\phi_b = 0$ if $V \leq V_{c1}$ or $V \geq V_{c2}$. Equation (A9) is always asymmetric with respect to V. This means that different permittivities (different grain orientations) and different donor densities are expected to result in asymmetric I–V behavior.

Although it may not be obvious at first glance, Eq. (A9) transitions into Eq. (A8) in the limes $\varepsilon_1 N_1 \to \varepsilon_2 N_2$. When substituting $a = Q_i + Q_{p1} + Q_{p2}$, $b = 2e\varepsilon_1 N_1$, and $c = V + p_i/\varepsilon_i$, Eq. (A8) can be written as

$$\phi_b = \begin{cases} eV + \dfrac{(a^2 - bc)^2}{4a^2 b} & \text{if } V \leq 0, \\ \dfrac{(a^2 - bc)^2}{4a^2 b} & \text{if } V \geq 0, \end{cases} \tag{A10}$$

and with $\xi = \frac{\varepsilon_2 N_2}{\varepsilon_1 N_1}$, $\varepsilon_1 N_1 \geq \varepsilon_2 N_2$, and rearranging, Eq. (A9) can be written as

$$\phi_b = \begin{cases} eV + \dfrac{a^4 + 2a^3\sqrt{\xi a^2 + (\xi - \xi^2)bc} + a^2(\xi a^2 + (\xi - \xi^2)bc)}{a^2 b\,(1-\xi)^2} & \text{if } V \le 0, \\ \dfrac{a^4 + 2a^3\sqrt{\xi a^2 + (\xi - \xi^2)bc} + a^2(\xi a^2 + (\xi - \xi^2)bc)}{a^2 b\,(1-\xi)^2} & \text{if } V \ge 0. \end{cases} \tag{A11}$$

This equation is not defined for $\xi = 1$, but by applying L'Hôpital's rule and with the condition $a < 0$ (which means that there must always be a net negative charge in the GB), we found a solution for the limit $\varepsilon_1 N_1 \to \varepsilon_2 N_2$,

$$\lim_{\xi \to 1} \frac{a^4 + 2a^3\sqrt{\xi a^2 + (\xi - \xi^2)bc} + a^2(\xi a^2 + (\xi - \xi^2)bc)}{a^2 b\,(1-\xi)^2} = \frac{(a^2 - bc)^2}{4a^2 b}, \tag{A12}$$

proving that Eq. (A8) is indeed a special case of Eq. (A9).

REFERENCES

[1]M. Matsuoka, Jpn. J. Appl. Phys. **10**, 736 (1971).
[2]G. E. Pike and C. H. Seager, J. Appl. Phys. **50**, 3414 (1979).
[3]G. Blatter and F. Greuter, Phys. Rev. B **33**, 3952 (1986).
[4]G. Blatter and F. Greuter, Phys. Rev. B **34**, 8555 (1986).
[5]F. Greuter and G. Blatter, Semicond. Sci. Technol. **5**, 111 (1990).
[6]Z. L. Wang and J. Song, Science **312**, 242, (2006).
[7]X. Wang, J. Zhou, J. Song, J. Liu, N. Xu, and Z. L. Wang, Nano Lett. **6**, 2768 (2006).
[8]Z. L. Wang, Adv. Mater. **19**, 889 (2007).
[9]J. H. He, C. L. Hsin, J. Liu, L. J. Chen, and Z. L. Wang, Adv. Mater. **19**, 781 (2007).
[10]Y. Zhang, Y. Liu, and Z. L. Wang, Adv. Mater. **23**, 3004 (2011).
[11]J. Zhou, Y. Gu, P. Fei, W. Mai, Y. Gao, R. Yang, G. Bao, and Z. L. Wang, Nano Lett. **8**, 3035 (2008).
[12]P. Keil, T. Frömling, A. Klein, J. Rödel, and N. Novak, J. Appl. Phys. **121**, 155701 (2017).
[13]N. Novak, P. Keil, T. Frömling, F. H. Schader, A. Martin, K. G. Webber, and J. Rödel, Acta Mater. **162**, 277 (2019).
[14]P. M. Verghese and D. R. Clarke, J. Appl. Phys. **87**, 4430 (2000).
[15]R. Baraki, N. Novak, T. Frömling, T. Granzow, and J. Rödel, Appl. Phys. Lett. **105**, 111604 (2014).
[16]R. Baraki, N. Novak, M. Hofstätter, P. Supancic, J. Rödel, and T. Frömling, J. Appl. Phys. **118**, 085703 (2015).
[17]N. Raidl, P. Supancic, R. Danzer, and M. Hofstätter, Adv. Mater. **27**, 2031 (2015).
[18]P. Keil, R. Baraki, N. Novak, J. Rödel, and T. Frömling, J. Phys. D: Appl. Phys. **50**, 175106 (2017).
[19]P. Keil, M. Trapp, N. Novak, T. Frömling, H.-J. Kleebe, and J. Rödel, Adv. Mater. **30**, 1705573 (2018).
[20]D. Bremecker, P. Keil, M. Gehringer, D. Isaia, J. Rödel, and T. Frömling, J. Appl. Phys. **127**, 034101 (2020).
[21]T. Billovits, B. Kaufmann, and P. Supancic, Open Ceram. **6**, 100125 (2021).
[22]J. Wong and F. P. Bundy, Appl. Phys. Lett. **29**, 49 (1976).
[23]T. K. Gupta, M. P. Mathur, and W. G. Carlson, J. Electron. **6**, 483 (1977).
[24]J. E. Schoutens and S. L. Senesac, J. Appl. Phys. **50**, 6283 (1979).
[25]H. Wang, W. Li, and J. F. Cordaro, Jpn. J. Appl. Phys. **34**, 1765 (1995).
[26]R. P. Rodrigues, J.-H.- Wang, and V. P. Dravid, J. Electroceram. **3**, 245 (1999).
[27]C. Cheng, J. He, and J. Hu, Appl. Phys. Lett. **101**, 173508 (2012).
[28]A. Nevosad, M. Hofstätter, P. Supancic, R. Danzer, and C. Teichert, J. Eur. Ceram. Soc. **34**, 1963 (2014).
[29]J. He, C. Cheng, and J. Hu, AIP Adv. **6**, 030701 (2016).
[30]H. Morko and Ü Özgür, *Zinc Oxide. Fundamentals, Materials and Device Technology* (Wiley-VCH, Weinheim, 2009).
[31]B.-X. Xu, Z.-Q. Zhou, P. Keil, and T. Frömling, AIP Adv. **8**, 115126 (2018).
[32]R. Einzinger, Appl. Surf. Sci. **3**, 390 (1979).
[33]C. Jagadish and S. J. Pearton, "Zinc oxide bulk, thin films and nanostructures," in *Processing, Properties and Applications* (Elsevier, Amsterdam, 2006).
[34]F. Greuter, in *Oxide Electronics*, edited by A. K. Ray (John Wiley & Sons, Inc., Hoboken, 2021), p. 157.
[35]K. Eda, J. Appl. Phys. **49**, 2964 (1978).
[36]M. Hayashi, M. Haba, S. Hirano, M. Okamoto, and M. Watanabe, J. Appl. Phys. **53**, 5754 (1982).
[37]F. Greuter, Solid State Ionics **75**, 67 (1995).
[38]C. Cheng, J. He, and J. Hu, Appl. Phys. Lett. **105**, 133508 (2014).
[39]B. Kaufmann, N. Raidl, and P. Supancic, J. Eur. Ceram. Soc. **40**, 3771 (2020).
[40]B. Kaufmann, T. Billovits, and P. Supancic, J. Eur. Ceram. Soc. **41**, 1969 (2021).
[41]B. Kaufmann, T. Billovits, M. Kratzer, C. Teichert, and P. Supancic, Open Ceram. **6**, 100113 (2021).
[42]E. H. Rhoderick, E. H. Rhoderick, and R. H. Williams, in *Metal-Semiconductor Contacts*, 2nd ed. (Clarendon Press, Oxford, 1988).
[43]Z. Zhang, V. Quemener, C.-H. Lin, B. G. Svensson, and L. J. Brillson, Appl. Phys. Lett. **103**, 072107 (2013).